

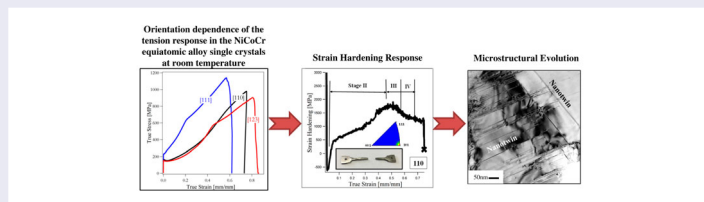
On the mechanical response and microstructure evolution of NiCoCr single crystalline medium entropy alloys

Benay Uzer^{a*}, S. Picak^{b,c*}, J. Liu^b, T. Jozaghi^c, D. Canadinc^{a,b}, I. Karaman^{b,c}, Y.I. Chumlyakov^d and I. Kireeva^d

^aDepartment of Mechanical Engineering, Koç University, Istanbul, Turkey; ^bDepartment of Materials Science and Engineering, Texas A&M University, College Station, Texas, USA; ^cDepartment of Mechanical Engineering, Texas A&M University, College Station, Texas, USA; ^dSiberian Physical Technical Institute, Tomsk State University, Tomsk, Russia

ABSTRACT

Unusual strain hardening response and ductility of NiCoCr equiatomic alloy were investigated through microstructural analysis of [111], [110] and [123] single crystals deformed under tension. Nano-twinning prevailed at, as early as, 4% strain along the [110] orientation, providing a steady work hardening, and thereby a significant ductility. While single slip dominated in the [123] orientation at the early stages of deformation, multiple slip and nanotwinning was prominent in the [111] orientation. Significant dislocation storage capability and resistance to necking due to nanotwinning provided unprecedented ductility to NiCoCr medium entropy alloys, making it superior than quinary variants, and conventional low and medium stacking fault energy steels.



IMPACT STATEMENT

A comparison of the current results on the ternary medium entropy alloy single crystals and those previously reported on the quinary and quaternary fcc equiatomic alloys demonstrates that a higher configurational entropy does not necessarily warrant improved mechanical properties.

ARTICLE HISTORY

Received 4 January 2018

KEYWORDS

Medium entropy alloys; multi-principal element alloys; single crystals; deformation twinning

Introduction

Material systems with multiple components, so-called high entropy alloys (HEAs) and medium entropy alloys (MEAs), have attracted recent attention owing to their high strength–ductility combination, and fracture toughness [1–9]. Moreover, these alloys exhibit unprecedented mechanical strength with high ductility levels, especially at cryogenic temperatures [4,5,10,11]. This exceptional mechanical behavior has been originally attributed to the solid solution strengthening where randomly distributed solid atoms exerts resistance to the dislocation glide, proposed to be in the amount proportional to the averaged mean-square atomic displacements [12]. However, a more recent study reported using neutron scattering experiments [13] that there is no direct indication of

anomalously large local lattice strains in HEAs, casting some doubts on the earlier solid solution strengthening arguments.

Equiatomic FeMnCrCoNi alloy is the first fcc HEA investigated in detail, and the microstructural origins of its mechanical response have recently been revealed [3,5,14,15]. Since the discovery of this five element HEA, many variations of other quinary, quaternary and ternary equiatomic multi-component alloys, having fcc, bcc and hcp structures, have been developed [7,8,10]. Among these, the studies on the various ternary and quaternary variants of transition metal fcc HEAs and MEAs showed that the NiCoCr MEA demonstrates the best combination of mechanical strength and fracture toughness among all fcc HEAs and MEAs investigated

CONTACT I. Karaman ikaraman@tamu.edu Department of Materials Science and Engineering, Texas A&M University, College Station, Texas 77843, USA

*These authors equally contributed in the preparation of the present manuscript.

© 2018 The Author(s). Published by Informa UK Limited, trading as Taylor & Francis Group.

This is an Open Access article distributed under the terms of the Creative Commons Attribution-NonCommercial License (<http://creativecommons.org/licenses/by-nc/4.0/>), which permits unrestricted non-commercial use, distribution, and reproduction in any medium, provided the original work is properly cited.

to date [4,16,17]. Its lower stacking fault energy (SFE) (22 ± 4 mJ/m², 25% lower than that of the FeMnCrCoNi, comparable to the SFE of Hadfield steel and 316 stainless steel) decreases the critical stress for twin formation [4,16], such that the necking instability is postponed and the ductility is enhanced. This is in good agreement with the fact that low SFE materials are more prone to deformation twinning [18], and thus, have increased strain hardening rates, dislocation storage capacity and ductility.

It has recently been shown that nanotwins forming in NiCoCr at the early stages of deformation promote high work hardening rates (WHRs) [4,16] since the twin boundaries hinder dislocation glide, similar to twinning-induced plasticity (TWIP) steels [19–22]. However, despite the promising results obtained on the polycrystalline NiCoCr, the underlying microstructural evolution in individual grain orientations and the effects of evolved microstructure on the mechanical properties have not been clearly understood. In order to address this issue, it is essential to distinguish the effects of grain and twin boundaries on the plastic deformation evolution. Therefore, the present study focused on the deformation response and microstructural evolution of the NiCoCr MEA in single crystalline form in order to examine the mechanical behavior as a function of crystallographic orientation, based on varying deformation mechanisms, including deformation twinning, dictated by the specific orientations. With this motivation, single crystalline NiCoCr samples oriented along the [110], [111] and [123] directions were subjected to uniaxial tension up to various strain levels, and microstructural evolution was monitored at different strain levels.

The rationale for the selection of these particular crystallographic orientations is to exemplify different regions of the stereographic triangle, the desire to form different number of slip and twinning systems at various stages of deformation, and to monitor the orientation dependence of the strain level at which twinning initiates and how twinning evolves. While multiple slip/twinning systems are expected in the [110] and [111] orientations, only one system should be activated in [123] at the early stages of deformation [6,21]. Furthermore, the propensity of twinning and slip with increasing deformation varies specific to crystallographic orientation. For instance, twinning is most favorable in the [111] and [110] oriented face-centered cubic (FCC) crystals since the Schmid factors for twinning ($m_{tw} = 0.314$ for [111] and 0.47 for [110]) are larger than that for slip ($m_{sl} = 0.27$ for [111] and 0.41 for [110]) [23]. Therefore, analysis of differently oriented samples can elucidate the effective mechanisms and their interactions governing the deformation response.

Experimental procedures

The equiatomic NiCoCr single crystals were grown using the Bridgman method in an argon atmosphere using the vacuum induction melted ingots. Dog-bone shaped tensile samples with dimensions of 8 mm × 3 mm × 1.5 mm in the gage section, and oriented along the [110], [111] and [123] crystallographic directions were cut from the bulk crystals by wire electric discharge machining. The samples were evacuated in quartz tubes, and then homogenized at 1473 K for 24 h, followed by water quenching.

Prior to experiments, X-ray diffraction (XRD) and electron backscatter diffraction (EBSD) were employed for phase identification and texture analysis. Elemental composition of the samples was quantified with wavelength dispersive X-ray spectroscopy (WDS). The samples analyzed with EBSD and WDS were final polished with colloidal silica suspension. Three samples in each orientation were subjected to tensile loading up to failure on a servo-hydraulic MTS frame at strain rate of 5×10^{-4} s⁻¹ at room temperature. Additional experiments were conducted by interrupting the tests at different strain levels in order to better understand the microstructural evolution at different stages of deformation. Surface relief on the sample surfaces was investigated with optical microscopy (OM), and the deformation activities were analyzed with a FEI Tecnai 20ST transmission electron microscope (TEM) operating at 200 kV. TEM samples were prepared by grinding the samples down to 60 μm thickness and punching them into 3 mm diameter discs, which were twin-jet electropolished at -20°C with an electrolyte consisting of 75% of methanol and 25% of nitric acid at 20 V.

The WDS analysis revealed that the samples contained almost equal atomic concentrations (in at. %) of Ni, Co and Cr: 33.42 ± 0.14 , 33.60 ± 0.68 and 32.98 ± 0.72 , respectively. In addition, XRD and EBSD analyses demonstrated that the single crystalline samples were shown to have a FCC structure with a lattice parameter of 0.3575 nm, which aligns well with the values reported in the literature [16,17,24].

Results and discussion

The stress–strain response of the samples deformed up to failure is presented in Figure 1(a). From these experiments and the results on the several companion samples for each orientation, the Young's modulus of each orientation is determined as: $E[111] = 375 \pm 32$ GPa, $E[110] = 300 \pm 28$ GPa and $E[123] = 280 \pm 35$ GPa. While the [110] and [123] orientations exhibit upper and lower yield strengths, and Lüder's type propagation

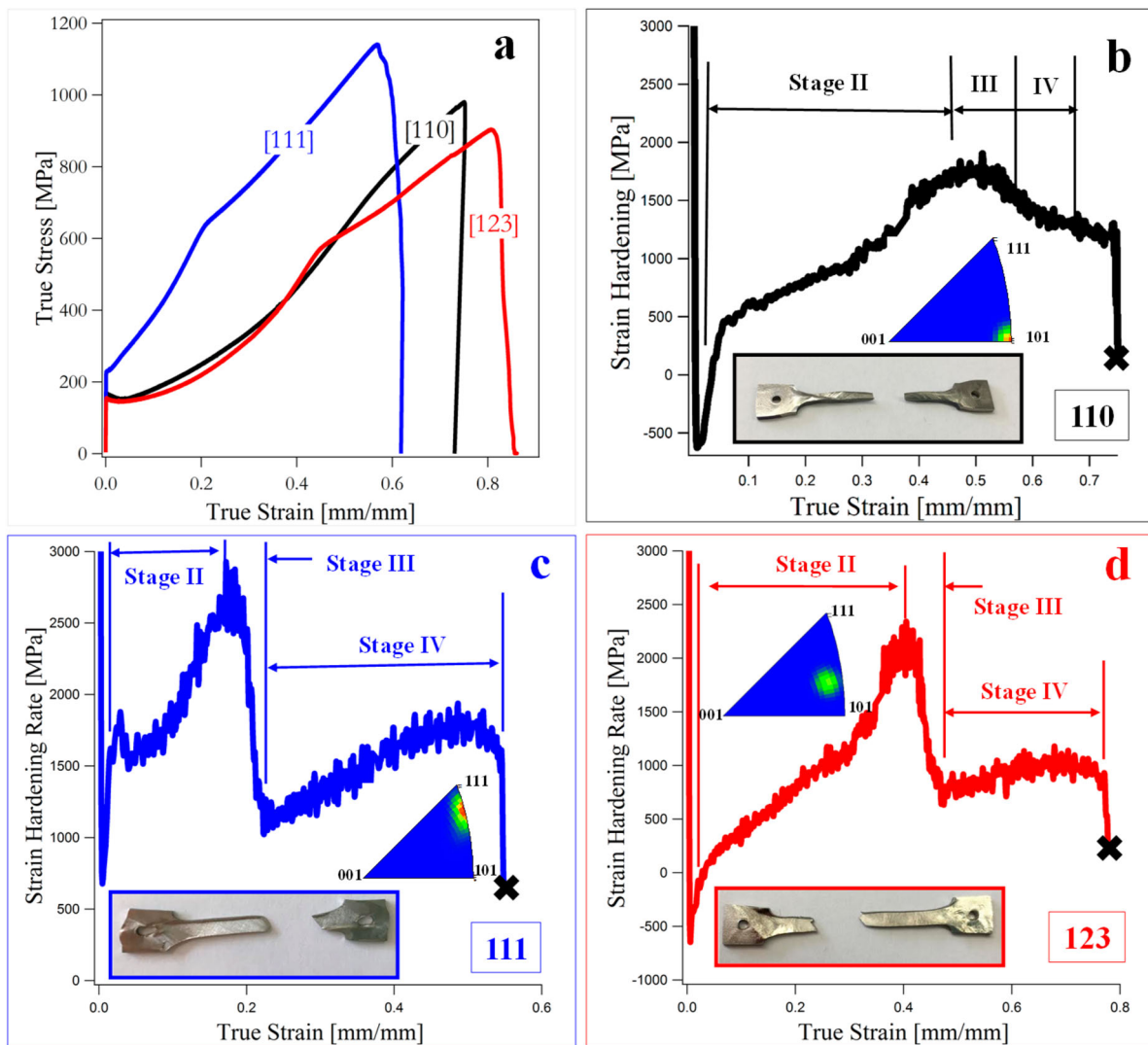


Figure 1. (a) True stress–true strain response of the NiCoCr medium entropy alloy single crystal samples oriented along the [110], [111] and [123] orientations deformed to failure under uniaxial tensile loading. Evolution of strain hardening rate as a function of true strain in the (b) [110], (c) [111] and (d) [123] orientations. The insets in (b), (c) and (d) exhibit the measured initial orientation of each crystal along the tensile axis.

of localized deformation, the [111] orientation demonstrates a linear hardening from the beginning of the deformation. This is associated with the different types and number of active deformation systems [25,26]: single deformation system prevails early in the [123] orientation, while multiple deformation systems are promoted in the [111] samples. Therefore, the [111] crystals do not exhibit extended stage I hardening region. The easy glide in the [123] samples leads to a low WHR in Stage I. In the [111] orientation, two or more active deformation systems interact with each other, leading to the start of Stage II deformation almost at the onset of plastic deformation. In the [110] direction, twinning nucleation causes Lüder's type propagation of deformation in Stage I.

The TEM images of the [110] sample deformed to 4% strain show planar dislocations on a single slip system

(Figure 2(a)) and the formation of two twin systems with a twin thickness of 1–2 nm (Figure 2(b)) on the {111} planes. Planar dislocation motion in this orientation is associated with the difficulty of cross slip due to low SFE and high resistance to cross slip imposed by the substitutional atoms [3]. At the early stages, plasticity takes place by the splitting of the $1/2\langle 110 \rangle$ type perfect dislocations into $1/6\langle 112 \rangle$ type Shockley partials. As a result of the coordinated glide of these partial dislocations on consecutive {111}-type planes, stacking faults are formed, which interact with the dislocations [27]. It should be noted that the formation of stacking faults in the early stages of plasticity of low SFE alloys contribute to the nucleation of twins by serving as precursors [26,28].

Activation of two different nanotwin systems, and their interactions with dislocations and stacking faults

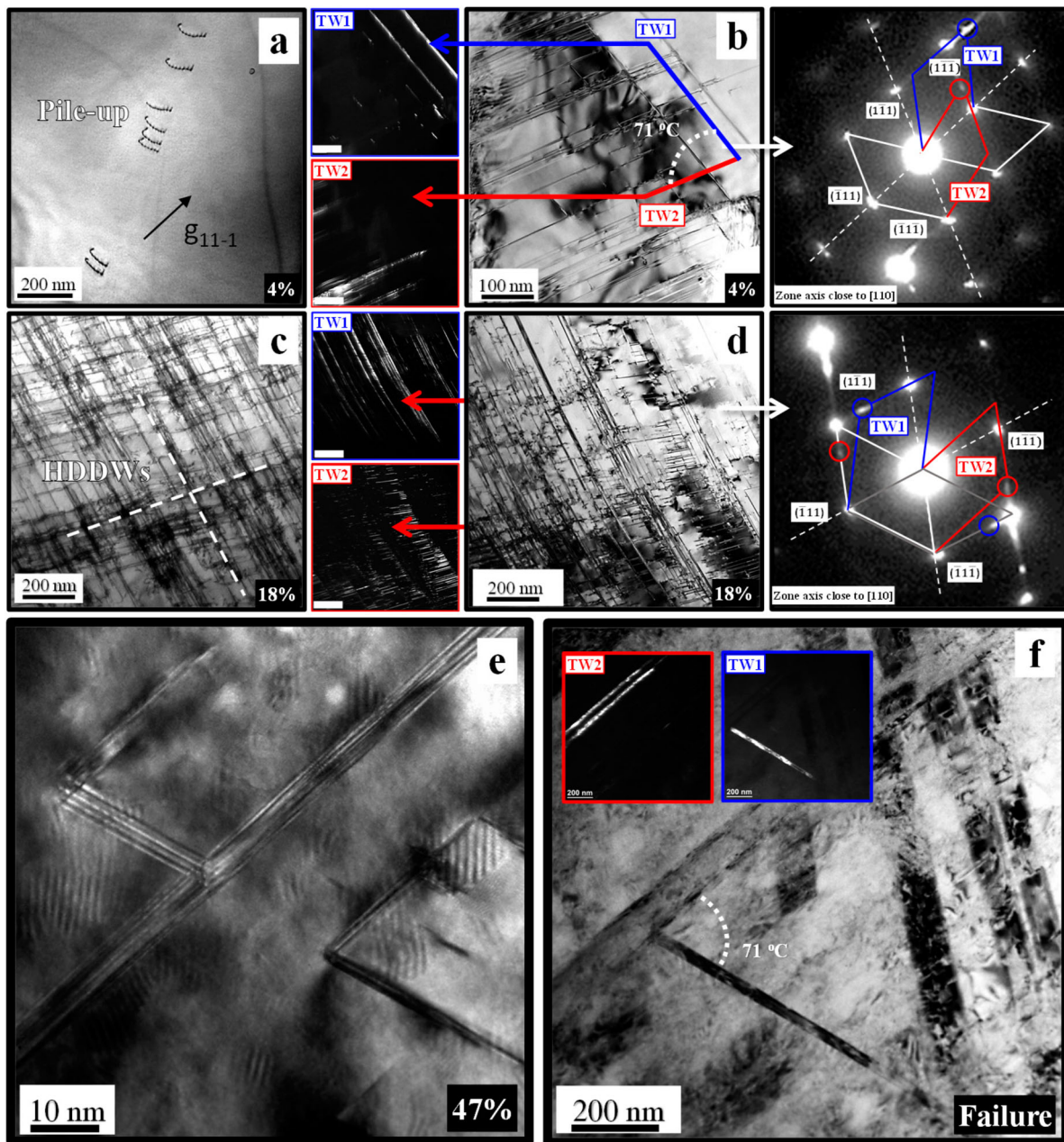


Figure 2. Bright field TEM images and corresponding diffraction patterns of the [110] oriented samples deformed up to ((a) and (b)) 4%, ((c) and (d)) 18%, (e) 47% and (f) failure.

promote an increased WHR in this sample following Stage I. Recently, nanotwin formation was reported to take place between 4.0 and 6.7% true strain in polycrystalline NiCoCr MEA subjected to tensile loading at 77 K [16]; however, to the best of the authors' knowledge, the present work is the first reporting the evidence of nanotwin formation at such small strains at room temperature in this material.

The strain hardening response of the [110] orientation in Stage II (Figure 1(b)) is primarily governed by multi-twin systems shown in Figures 2(b,d). The sharp increase

in strain hardening curve in Stage II in Figure 1(b) is associated with twin boundaries where they act as barriers to dislocation motion [21]. Moreover, TEM image of the [110] sample deformed to 18% revealed a second slip system interacting with the primary one (Figure 2(c)). The interaction of the slip systems forms the carpet structure (Figure 2(c)), which is commonly observed in low SFE materials [25], such as 316L stainless steel [28]. Increase of dislocation density concomitant with plastic deformation gives rise to the rows of positive and negative edge dislocations, increasing the stress [25]. Once

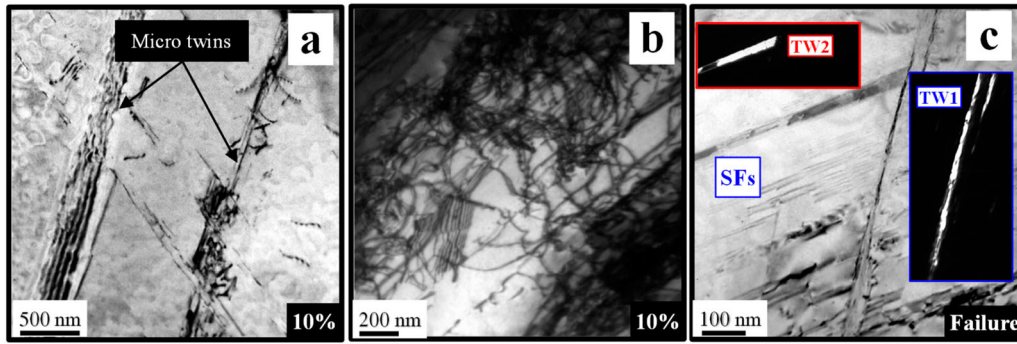


Figure 3. TEM images and diffraction patterns of the [111] oriented samples deformed up to (a)–(b) 10% and (c) failure.

a critical stress value is achieved, these dislocation multipoles, which block the initial slip plane, promote dislocation activity on fresh slip planes in order to accommodate the imposed strain. The initiation of dislocation glide on interacting systems creates these carpet structures [25], eventually leading to high density dislocation walls (HDDWs) [29]. The twin density also increases in Stage II (Figure 2(d)), ultimately decreasing the mean free path (MFP) of the dislocations and enhancing dislocation storage [28]. Twin boundaries impede dislocation glide, a phenomenon known as dynamic Hall-Petch effect, which increases the WHR. Overall, the strain hardening in Stage II in the [011] orientation is strongly influenced by deformation twinning and HDDWs since they act as a strong obstacles to dislocation motion by reducing dislocation MFP.

An additional increase in Stage II hardening (max $\text{WHR} = G/45$, where G is the shear modulus) is clear at the later stage of the deformation in Figure 1(b), the reason of which was investigated using TEM in the [110] sample deformed to 47% of strain. As shown in Figure 2(e), notable amount of stacking faults were observed on multiple {111} planes, forming so-called parallelepipeds [13]. The interaction of stacking faults gives rise to the formation of these parallelepipeds, which act as additional barriers to dislocation motion, and further increase the strain hardening rate. Stage II hardening is followed by Stage III where dislocation recovery takes place leading to reduction in strain hardening coefficient. Stage III is then interrupted by Stage IV hardening where more twinning activity takes place. At Stage IV, the thicknesses of the pre-existing and the newly formed twins increase, facilitating interactions with each other and existing dislocation substructure (Figure 2(f)). These changes in the twin activity result in further increase in ductility, since they suppress deformation localization and necking.

Similar to the [110] samples, stress–strain response of [111] samples can be divided into clearly distinguishable

four stages (Figure 1(c)). In order to understand the governing mechanisms in the early stages of plastic deformation, the sample was deformed to 10% strain. The TEM image in Figure 3(a) shows the activation of twinning and twin/slip interaction, which provides a high WHR throughout Stage II (with a maximum of $G/30$). Through the activation of multi-slip systems, dislocation tangles and multipoles (Figure 3 (b)) are formed in the early stages of deformation. The dislocations on primary and conjugate slip systems form the Lomer–Cottrell locks, which involves the sessile dislocation configuration blocking slip [21]. Specifically, the interaction of partial dislocations with the Lomer–Cottrell locks increases local stress concentration, facilitating the formation of additional deformation twins at the later stages of deformation [27]. The mutual interaction of these mechanisms promotes the strengthening of the material and provide the high WHR in the deformation stage II.

In the [111] orientation, following Stage II, Stage III deformation takes place where dislocation recovery occurs causing a decrease in strain hardening rate from $G/30$ to $G/65$. However, the decrease in WHR in Stage III is terminated with the start of Stage IV due to the well-known TWIP effect [29]. In order to elucidate the dominant deformation mechanisms at later deformation stages, the [111] orientation was deformed up to failure: two active twin systems with the average thicknesses of 20 and 30 nm were observed and the thicker twins block the propagation of the thinner ones (Figure 3(c)). These nanotwins also interact with the stacking faults and dislocations, delaying the onset of necking and thereby increasing the ductility [4]. The above observations about the propensity of twins in this alloy are also supported by a recent study, where the twinnability of this alloy was reported to be higher than all pure FCC metals and comparable to that of the Fe–Cr–Ni TWIP steels [30].

Stage I deformation in the [123] orientation is governed by single planar slip system which leads to low

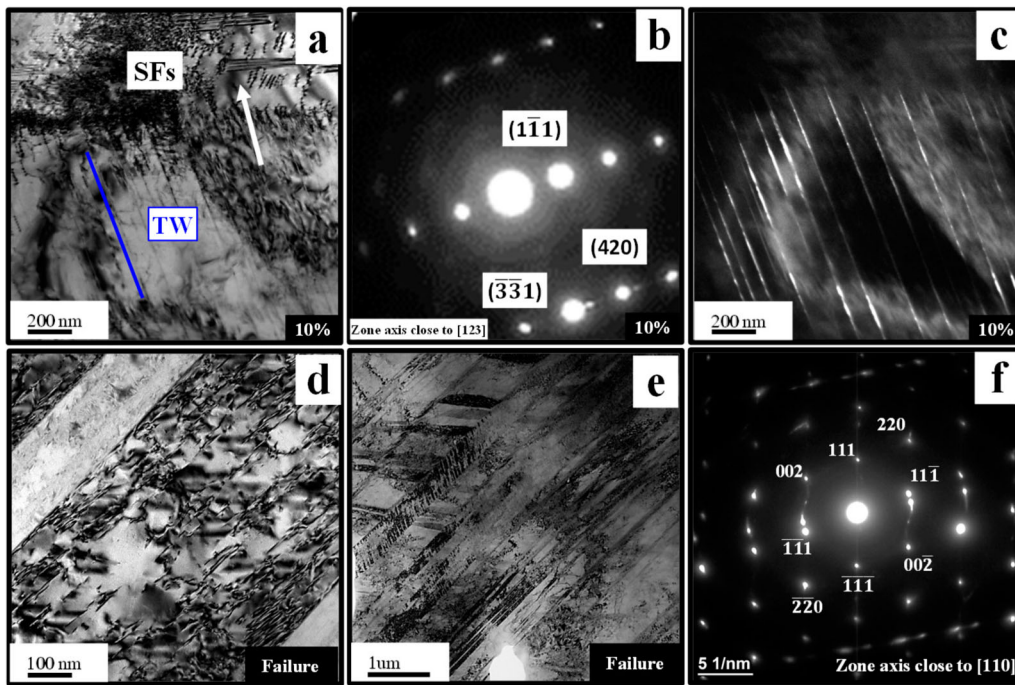


Figure 4. TEM images and diffraction patterns of the [123] oriented samples deformed up to (a)–(c) 10% and (d)–(f) failure.

hardening. However, the nanotwins observed in the [123] samples deformed to 10% (see Figures 4(a–c)) bring about a sharp increase in WHR, similar to the [111] and the [110] oriented samples. In addition, twin–slip interaction causes an increase in strain hardening rate through Stage II. The transition from Stage II to Stage III (max WHR = $G/40$) represents dislocation recovery

stage similar to the behavior in the [110] and [111] orientations. This stage ended at WHR = $G/80$ due to the formation of new twin systems, similar to those observed in TWIP steels [31], representing the onset of Stage IV (Figure 1(d)). The activation of multiple twin systems in the Stage IV deformation of the [123] orientation creates a 3D twin network (Figure 4(e)), which offers

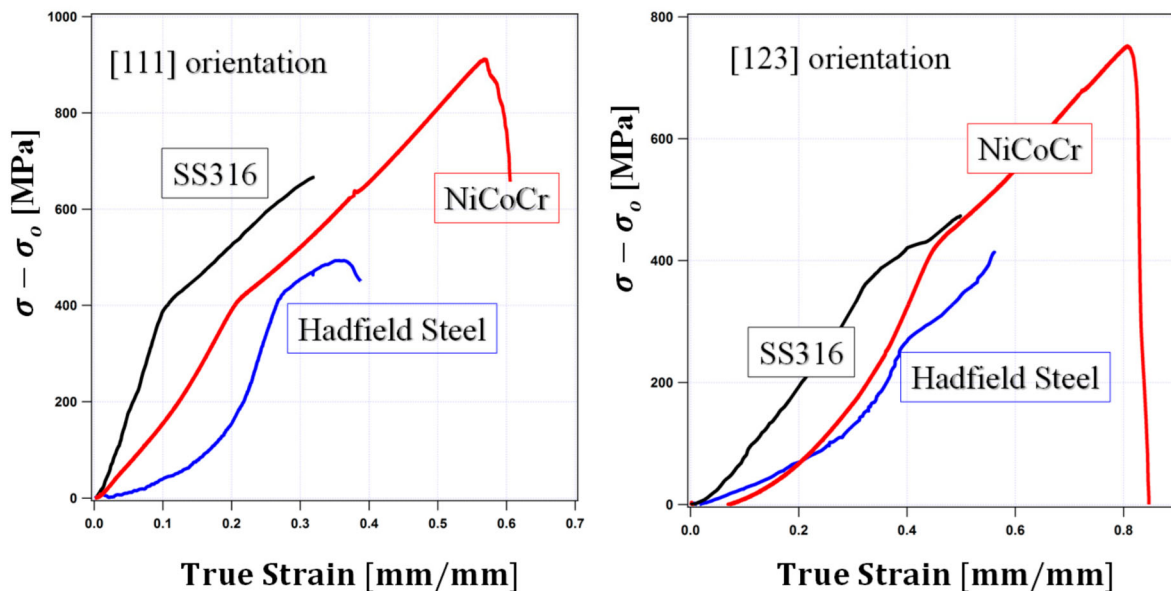


Figure 5. Comparison of the strength differentials ($\sigma - \sigma_0, \sigma_0$: Yield strength) and hardening response as a function of the applied strain in three different medium to low stacking faculty energy materials: 316 stainless steel (SS316) [28], Fe-12%Mn-1%C Hadfield steel [21] and the present medium entropy NiCoCr alloy, indicating superior ductility and strength differential in the NiCoCr alloy.

multiple pathways for the dislocation motion [30] and more boundaries for dislocation storage, enhancing the ductility of the material and delaying the onset of necking. Furthermore, formation of dislocation cells between the twin lamellae (Figure 4(d)) in the [123] orientation creates dislocation-free regions, promoting easy glide, similar to what was observed in 316L stainless steel single crystals [28].

Based on the above observations, we attempted to calculate the critical resolved shear stresses (CRSS) for slip and twinning in the NiCoCr MEA by assuming that in all three orientations the onset of plastic deformation (i.e. yield strength) occurred due to dislocation slip, and twinning has started in the [110] orientation at a strain level around 4% and in the [111] and [123] orientations below 10%. Based on these assumptions, the CRSS for slip was found to be 69 ± 3 MPa and the CRSS for twinning was determined to be 78 ± 5 MPa.

It should be noted that the uniaxial tensile responses of three orientations of equiatomic NiCoCr MEA single crystals investigated here is quite similar to those observed in 316L stainless steel [28] and Fe-12%Mn-1%C Hadfield steel [21] single crystals, in terms of the hardening response, stages of the deformation, and relative hardening rates. The main differences between this MEA and the latter steels are that the steels exhibit higher yield strengths (i.e. their CRSS are higher than that of the NiCoCr MEA), however, the NiCoCr MEA crystals demonstrate much higher ductility, i.e. more than 50% higher (Figure 5). The main difference between NiCoCr MEA and 316 stainless steel/Hadfield steel single crystals is the extent of Stage IV hardening in the orientations studied (i.e. [111], [123] and [110]). In NiCoCr single crystals the total strain levels for combined stage III and stage IV are significantly more than those in both 316 stainless steel and Hadfield steel (Figure 5). This indicates that the secondary twinning and/or twin networks are quite effective in Stage IV deformation of NiCoCr crystals in suppressing necking and increasing the ductility. One potential reason is that the twins in NiCoCr seem to be thinner than 316 stainless steel and Hadfield steel in Stage IV, probably providing more boundaries for slip to interact. This indicates that dislocation storage capability and resistance to necking instability of NiCoCr should be better than these conventional low and medium SFE steels.

Summary and conclusions

The findings presented herein demonstrate that the superior mechanical properties of NiCoCr MEA are strongly orientation dependent. More importantly, nanotwin formation was shown to start as early as 4% strain,

contributing to the significant ductility by promoting a steady work hardening response and postponing necking. Multi-twin systems were observed in all three orientations studied here at different strain levels. Furthermore, the current results also imply that a higher configurational entropy does not necessarily warrant improved mechanical properties, as in the case of the NiCoCr MEA as compared to its HEA counterparts. Overall, the current findings shed light on the complicated microstructural evolution and strain hardening response of NiCoCr MEAs.

Acknowledgements

BU acknowledges the help of Hande Ozcan in performing some of the experiments. DC and BU acknowledge the support of Koç University, Graduate School of Sciences and Engineering.

Disclosure statement

No potential conflict of interest was reported by the authors.

Funding

This research was supported by the Chevron Professorship at Texas A&M University. Y.I.C acknowledges the support by Russian Science Foundation (RSF) [grant no. 16-19-10193].

ORCID

I. Karaman  <http://orcid.org/0000-0001-6461-4958>

References

- [1] Yeh BJ, Chen S, Lin S, et al. Nanostructured high-entropy alloys with multiple principal elements: novel alloy design concepts and outcomes. *Adv. Eng. Mat.* **2004**;6:299–303.
- [2] Cantor B, Chang ITH, Knight P, et al. Microstructural development in equiatomic multicomponent alloys. *Mater Sci Eng A.* **2004**;375–377:213–218.
- [3] Kireeva I, Chumlyakov Y, Pobedennaya ZV, et al. Slip and twinning in the [-149] oriented single crystals of a high-entropy alloy. *Russ Phys J.* **2016**;59:1242–1250.
- [4] Gludovatz B, Hohenwarter A, Thurston KVS, et al. Exceptional damage-tolerance of a medium entropy alloy CrCoNi at cryogenic temperatures. *Nat Commun.* **2016**;7:10602.
- [5] Gludovatz B, Hohenwarter D, Catoor EH, et al. A fracture-resistant high-entropy alloy for cryogenic applications. *Science.* **2014**;345:1153–1158.
- [6] Kireeva IV, Chumlyakov YI, Pobedennaya ZV, et al. Orientation dependence of twinning in single crystalline CoCrFeMnNi high entropy alloy. *Mat Sci Eng A.* **2017**;705:176–181.
- [7] Miracle DB, Senkov ON. A critical review of high entropy alloys and related concepts. *Acta Mater.* **2017**;122:448–511.
- [8] Wu Z, Bei H, Otto F, et al. Recovery, recrystallization, grain growth and phase stability of a family of

- FCC-structured multi-component equiatomic solid solution alloys. *Intermetallics*. **2014**;46:131–140.
- [9] Otto F, Dlouhy A, Somsen C, et al. The influences of temperature and microstructure on the tensile properties of a CoCrFeMnNi high-entropy alloy. *Acta Mater*. **2013**;61:5743–5755.
- [10] Gali A, George EP. Tensile properties of high- and medium-entropy alloys. *Intermetallics*. **2013**;39: 74–78.
- [11] Otto F, Yang Y, Bei H, et al. Relative effects of enthalpy and entropy on the phase stability of equiatomic high-entropy alloys. *Acta Mater*. **2013**;61:2628–2638.
- [12] Okamoto NL, Yuge K, Tanaka K, et al. Atomic displacement in the CrMnFeCoNi high-entropy alloy—A scaling factor to predict solid solution strengthening. *AIP Advances*. **2016**;6:125008.
- [13] Owen LR, Pickering EJ, Playford HY, et al. An assessment of the lattice strain in the CrMnFeCoNi high-entropy alloy. *Acta Mater*. **2017**;122:11–18.
- [14] Laplanche G, Kostka A, Horst OM, et al. Microstructure evolution and critical stress for twinning in the CrMnFeCoNi high-entropy alloy. *Acta Mater*. **2016**;118: 152–163.
- [15] Wu Z, Bei H, Pharr GM, et al. Temperature dependence of the mechanical properties of equiatomic solid solution alloys with face-centered cubic crystal structures. *Acta Mater*. **2014**;81:428–441.
- [16] Laplanche G, Kostka A, Reinhart C, et al. Reasons for the superior mechanical properties of medium-entropy CrCoNi compared to high-entropy CrMnFeCoNi. *Acta Mater*. **2017**;128:292–303.
- [17] Jin K, Gao YF, Bei H. Intrinsic properties and strengthening mechanism of monocrystalline Ni-containing ternary concentrated solid solutions. *Mater Sci Eng A*. **2017**;695: 74–79.
- [18] Zhao YH, Zhu YT, Liao XZ. Tailoring stacking fault energy for high ductility and high strength in ultra-fine grained Cu and its alloy. *Appl Phys Lett* **2006**;89: 121906.
- [19] Gumus B, Bal B, Gerstein G, et al. Twinning activities in high-Mn austenitic steels under high-velocity compressive loading. *Mater Sci Eng A*. **2015**;648:104–112.
- [20] Miao J, Slone CE, Smith TM. The evolution of the deformation substructure in a Ni-Co-Cr equiatomic solid solution alloy. *Acta Mater*. **2017**;132:35–48.
- [21] Karaman I, Sehitoglu H, Gall K, et al. Deformation of single crystal Hadfield steel by twinning and slip. *Acta Mater*. **2000**;48:1345–1359.
- [22] Karaman I, Sehitoglu H, Chumlyakov YI, et al. The deformation of low-stacking-fault-energy austenitic steels. *JOM*. **2002**;54:31–37.
- [23] Kireeva IV, Chumlyakov YI. Effect of nitrogen and stacking-fault energy on twinning in [-111] single crystals of austenitic stainless steels. *Phys Met Metallogr*. **2009**;108(3): 298–309.
- [24] Zhang FX, Zhao S, Jin K, et al. Local structure and short-range order in a NiCoCr solid solution alloy. *Phys Rev Lett*. **2017**;205501:1–6.
- [25] Kuhlmann-Wilsdorf D. Theory of plastic deformation: - properties of low energy dislocation structures. *Mater. Sci. Eng. A*. **1989**;113:1–41.
- [26] Canadinc D, Sehitoglu H, Maier HJ, et al. Orientation evolution in Hadfield steel single crystals under combined slip and twinning. *Int J Solids Struct* **2007**;44:34–50.
- [27] Choi WS, Sandlöbes S, Malyar NV, et al. Dislocation interaction and twinning-induced plasticity in face-centered cubic Fe-Mn-C micro-pillars. *Acta Mater*. **2017**;132:162–173.
- [28] Karaman I, Sehitoglu H, Maier HJ, et al. Competing mechanisms and modeling of deformation in austenitic stainless steel single crystals with and without nitrogen. *Acta Mater*. **2001**;49:3919–3933.
- [29] Canadinc D, Sehitoglu H, Maier HJ, et al. Strain hardening behavior of aluminum alloyed Hadfield steel single crystals. *Acta Mater*. **2005**;53:1831–1842.
- [30] Zhang Z, Sheng H, Wang Z, et al. Dislocation mechanisms and 3D twin architectures generate exceptional strength-ductility-toughness combination in CrCoNi medium-entropy alloy. *Nat Commun* **2017**;8:14390.
- [31] Barbier D, Gey N, Allain S, et al. Analysis of the tensile behavior of a TWIP steel based on the texture and microstructure evolutions. *Mater. Sci. Eng. A*. **2009**;500:196–206.